Letters on Materials 15 (4), 2025 pp. 431-439 www.lettersonmaterials.com

Received 1 October 2025; Accepted 28 November 2025 https://elibrary.ru/xvgjlo
https://doi.org/10.48612/letters/2025-4-431-439

Effect of the height of welding tip teeth on the structure and strength of Cu/Cu joints produced by spot ultrasonic welding

E. R. Shayakhmetova, M. A. Murzinova†, A. A. Nazarov

†mma@imsp.ru

Institute for Metals Superplasticity Problems, Russian Academy of Sciences, Ufa 450001, Russia

Abstract: Spot ultrasonic welding (USW) of metals is used in mass production to join thin metal plates and/or wires and robustness of the welding process and minimizing the variation in quality characteristics of the joints are important factors. The joint quality depends on a number of factors including the design of welding tool. In this study, tools with tooth heights of 0.1 and 0.4 mm were used to produce spot welds of 0.8 mm-thick copper plates. The effect of tool tooth height on the quality of the welded samples was estimated based on a comparison of their linear weld density (LWD), normal strains in the weld spot, microstructure of samples, as well as the strength characteristics. It was established that tooth height has a weak effect on the LWD which correlates with compressive strains in the weld spot and achieves about 40% under tooth imprints. More importantly, the distance between the areas of high weld density is half as much after USW with the tool with fine teeth than after USW with the tool with coarse teeth. Regardless of the selected welding tool fine grains form in the joint zone and submicrometer-sized pores present between the fine grains. USW with a tool with coarse teeth was accompanied with an increase in fraction of area occupied by fine grains and formation of regions with mechanical interlocking of material in joint zone. The average fracture loads of weld samples obtained using the tools with different tooth heights are similar and amount to approximately 2000 N. However, the variation coefficient of the test results is by a factor of 2.4 smaller after ultrasonic welding using the tool with fine teeth. Thus, optimizing the knurl height of flat welding tools can be an effective method for improving the stability of properties of ultrasonically welded joints.

Keywords: ultrasonic welding, copper, microstructure, interface temperature, joint quality

Acknowledgements *This work was carried out within the state assignment of IMSP RAS (No. 124022900006-2). Part of experimental data was obtained during the accomplishment of a project supported by the Russian Science Foundation (grant #22-19-00617, https://rscf.ru/project/22-19-00617/). Electron microscopic studies and mechanical tests were carried out on the facilities of shared services center of IMSP RAS "Structural and Physical-Mechanical Studies of Materials".*

1. Introduction

The performance properties of welded metal joints depend on their structure, which is formed during the welding process. Fusion welding results in the formation of a structure typical of casts in a joint, significant grain growth in a thermomechanically affected zone [1], the appearance of pores due to the interaction of metal with air, and cracks as a result of thermal shrinkage strains [2]. Solid-state welding processes are free from the aforementioned drawbacks; however, their use also results in structural changes in joined metals, which are caused by the effects of temperature and/or deformation. Unlike pressure welding, linear and rotary friction welding, and friction stir welding, during the use of which the temperature in a joint zone typically reaches $(0.7-0.9)T_m$, where T_m is the melting point, the temperature in the process of ultrasonic welding (USW) of metals rarely exceeds $0.5T_m$ [3,4]. During USW, material at a weld spot is subjected to the simultaneous action of normal and high-speed alternating shear strains. The quality of joints, i.e., the area fraction of defect-free regions and, consequently, electrical resistance, short-term strength, and fatigue strength, depend on the distribution of temperature and strains. It has been shown that even after careful optimization of USW parameters (vibration amplitude, clamping pressure, and input energy), the joint strength remains below the properties of the base materials under joining, and the results of mechanical tests of joints vary significantly [5–7]. This is a crucial problem requiring solution, since USW is used in mass production to join thin metal plates and/or wires in the manufacture of household appliances, batteries, in the automotive industry, etc. [8]. For such industries, robustness of the welding process and minimizing the variation in quality characteristics of the joints are important factors.

It has been shown that the robustness of the properties of welded joints produced by USW depends not only on the process parameters and the quality of surface preparation of the plates/wires being joined, but also on the design features of the welding tool, such as the shape of the welding tip (flat, cylindrical, or spherical) [9–11] and the relative positions of knurls on working surfaces of the tool [12].

A tool for USW of thin metal plates consists of a welding tip and an anvil. The anvil serves as a support for the parts being welded and is designed to fix the position of the bottom plate (substrate). The tip transmits ultrasonic energy and static clamping force to the workpieces being joined. In ideal configurations considered in simulation studies [13–15], the welding tip is considered to be rigidly connected to the top plate being welded. Therefore, the tip does not slip along the latter and the plate performs reciprocating movements relative to the stationary bottom plate rigidly connected to the anvil. In this ideal case, heat is generated only on the surfaces being welded, which facilitates the formation of the joint. In real conditions, slippage of the tip along the surface of the top plate cannot be eliminated, however [15–18]. Therefore, heat is generated not only on the surfaces being welded, but also on the contact surfaces of the tool with the plates [15,19–22]. This leads to losses of the supplied energy and accelerated wear of the tool. To avoid slippage between the tool and plates and, correspondingly, these losses, knurls are made on the surfaces of the tip and the anvil, usually in the form of trapezoidal or pyramidal teeth. In modern USW technologies, flat tools with a knurl height of 0.15–1.25 mm are normally used to obtain spot welds of metal plates [23–25]. It has been shown that extrusion of metal into the valleys between ridges can be accompanied by the appearance of tensile strains in localized areas of joints, which leads to a catastrophic increase in the relative length of discontinuities in these areas [12,21,26,27]. A way for ensuring compressive strains necessary for defect healing is complete filling of the valleys with metal [28]. Obviously, such filling can be facilitated by a reduction in the height of knurls. At the same time, such a reduction can affect the heat generation in plates during USW, the strain of the specimens at the weld spot, and eventually the structural changes in the bulks of plates and in the joint zone.

The present study aims to evaluate the effect of the tooth height of welding tool on the quality of lap spot welds of copper plates. To achieve this goal, we conducted a comparative study of the structure, distributions of normal strain and linear weld density, as well as the strength characteristics of the joints obtained under identical conditions of ultrasonic spot welding of 0.8 mm thick copper plates using welding tools with tooth heights of 0.1 and 0.4 mm.

2. Material and methods

Rectangular-shaped plates (50 mm × 20 mm) were cut from a sheet of commercially pure copper (99.96 wt.%) with a thickness of 0.8 mm. The average grain size in the cross-section of the sheet perpendicular to the rolling direction was 9.8 ± 0.4 μm. In the misorientation spectrum, the fraction of high-angle boundaries (HABs) reached 90–95%, and about 40–45% of the HABs were twin boundaries Σ3. Detailed description of this structure was given in our previous work [29] and additional information will be presented in Section 3.2. The specimens were ground using P240 sandpaper and washed in ethanol. USW was performed using laboratory equipment manufactured at the Institute for Metals Superplasticiy Problems, Russian Academy of Sciences (Russia). The process parameters used during USW are shown in Table 1. Two flat tips with dimensions of 6 mm × 6 mm were used. The tips had knurls in the form of trapezoids, one with a height of $H = 0.1$ mm (fine teeth) and the other with a height of $H = 0.4$ mm (coarse teeth). Each tip was used with an anvil whose working surface had teeth of the same height as the those of the welding tip (Fig. 1a). Spot USW produced samples schematically shown in Fig. 1b. During welding, the temperature in the joint zone was measured. For this purpose, a groove was machined in the bottom plate, into which a 0.5 mm diameter chromel-alumel thermocouple was inserted (Fig. 1b).

Using each tool, 6 to 7 joint samples were produced. At least five of these were subjected to tensile lap-shear testing on an Instron 5982 universal testing machine (England). Testing was conducted at room temperature with a crosshead speed of 1 mm/min. Average values of the peak loads were calculated from the test results as fracture forces. The standard deviation was taken as the measure of the random scatter, i. e.,

Table 1. The process parameters used during ultrasonic welding process.

Welding parameters	Values
Frequency (kHz)	20
Vibration amplitude (μm)	18–20
Clamping force (kN)	2.5
Ultrasound exposure (s)	3

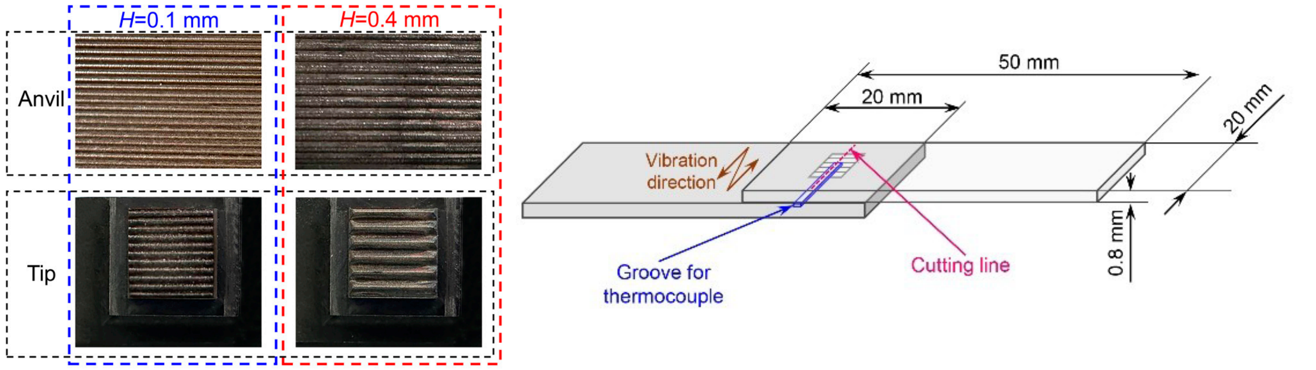

Fig. 1. (Color online) Photographs of welding tools (a); schematic illustration of a welded sample with a groove for a thermocouple when measuring temperature (b).

measurement error. Changes in the strength properties of copper plates caused by USW were characterized using Vickers microhardness (HV) measurements. The measurements were performed on an ITV-1AM microhardness tester (Russia). The load of 0.098 N (10 gf) and loading time of 10 s were used. The measurements were performed on cross-sections of the initial sheet and welded samples prepared for structural studies (see below). An average microhardness value was determined from seven measurements. The standard error was taken as the statistical error.

The structure of the welded samples was examined in cross-sectional planes passing through the centers of the weld spots parallel to the vibration direction, as shown in Fig. 1b (see dash-dotted pink line). Samples for microstructural observations were mechanically ground with SiC sandpaper and then polished with a suspension of colloidal silicon with a grain size of 0.05 μm. Microstructure studies were performed on a MIRA 3 LMH scanning electron microscope (Tescan, Czech Republic) at a voltage of 20 kV in backscatter electron (BSE) mode. Magnification ranged from ×20 to ×15 000. Structural analysis of the samples was also carried out using electron backscatter diffraction (EBSD). EBSD mapping was performed with a step size of 0.2 μm. Details of the EBSD data acquisition and treatment have been described in our previous study [30]. Channel 5 software was used to obtain quantitative characteristics of the microstructure. Quantitative analysis of the microstructure was carried out in accordance with the requirements of ASTM E112-10.

The values of the normal strain of weld spot e_{ni} (%) and linear weld density LWD_i (%) in a central cross-section of a specimen were determined under imprints of each tooth and valley of the welding tip using the formulas $e_{ni}=100\times(h_i-h_0)/h_0$, where h_i is the cross-section thickness of the welded specimen in the selected location, h_0 is the double thickness of the initial sheet, and $\mathrm{LWD}_i=100\times L_w/L_i$, where L_i and L_w are the lengths of the entire weld line and the defect-free section of the weld in the selected location, respectively. The measurements of h_0 and h_i were performed on an instrumental microscope at a magnification of ×30, and the values of L_i and L_w were measured in the ImageJ program on BSE images obtained at a microscope magnification of ×1000. The method of measuring normal strains and LWD was described and illustrated in detail in [12].

3. Results and discussion

3.1. Temperature, normal strains and linear weld density

USW for 3 s using the tools with tooth heights of $H=0.1$ and 0.4 mm resulted in a temperature increase in the joint zone to 321±19 and 268±21°C, respectively (Fig. 2), which amount to approximately $(0.45-0.4)T_m$ for copper. Therefore, the material in the weld spot zone was subjected predominantly to warm deformation during USW [31,32]. The strains during USW consist of normal and shear ones [25]. The high-rate alternating shear strains are concentrated near the contact surfaces of the plates and decrease towards the surfaces of plates in contact with the tool. The magnitude of shear strains depends on the thickness of plates and amplitude of their displacements, the latter in turn is related to the amplitude of the tip displacements [18,25]. Since the thickness of the plates and amplitude of the tip displacements were the same in the experiments, it can be assumed that the magnitudes of the accumulated shear strain were similar after welding with the tools with different tooth heights.

Normal strains, on the other hand, depend significantly not only on the clamping force, which was unchanged in the experiments, but also on the periodicity of the tool teeth and the depth of their penetration into the joined plates (Fig. 3). According to [13,21,33], the magnitude of normal strains is greatest in the contact zones of the welded plates with the tool and lowest at the joint surface. After USW using the tool with $H=0.4$ mm, depending on the relative positions of the anvil and tip teeth, both compressive and tensile normal strains were recorded at the weld spot [12]. On contrary, only compressive strains were observed at the weld joints obtained by USW using the tool with $H=0.1$ mm. Therefore, in this study, we deliberately compare the linear weld density and microstructure at weld spots where, after USW with different tools, only compressive normal strains were recorded. It is evident that the normal strains at a weld spot vary periodically. The period of change is equal to the distance between the tip tooth peaks and is almost half as much after welding with the tool with fine teeth (Fig. 3). After welding with different tools, the greatest compressive strains were observed under the tip tooth imprints and were similar in magnitude, approximately 12–14%. Under the tip valleys, compressive strains were smaller and amounted to approximately 3 and 9%, respectively, after USW with the tools with 0.1 and 0.4 mm tooth heights. In both cases, a correlation was observed between the values of local strain and the LWD of the joints. After USW using the tool with $H=0.1$ mm, the value of LWD under the imprints of tip teeth and between them (under the valleys between the teeth) varied from 44 to 15% with the average value of 31% over the joint line. After USW using the tool with $H=0.4$ mm, the LWD varied from 50 to 20%, and its average value was 37%.

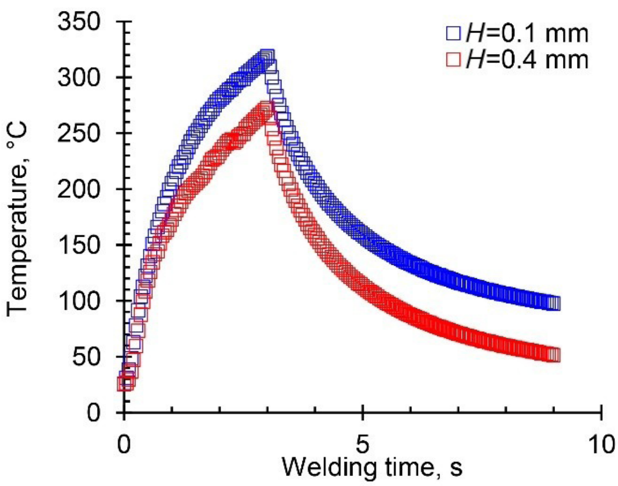

Fig. 2. (Color online) Typical dependencies of the temperature on time during USW of copper plates with different tools.

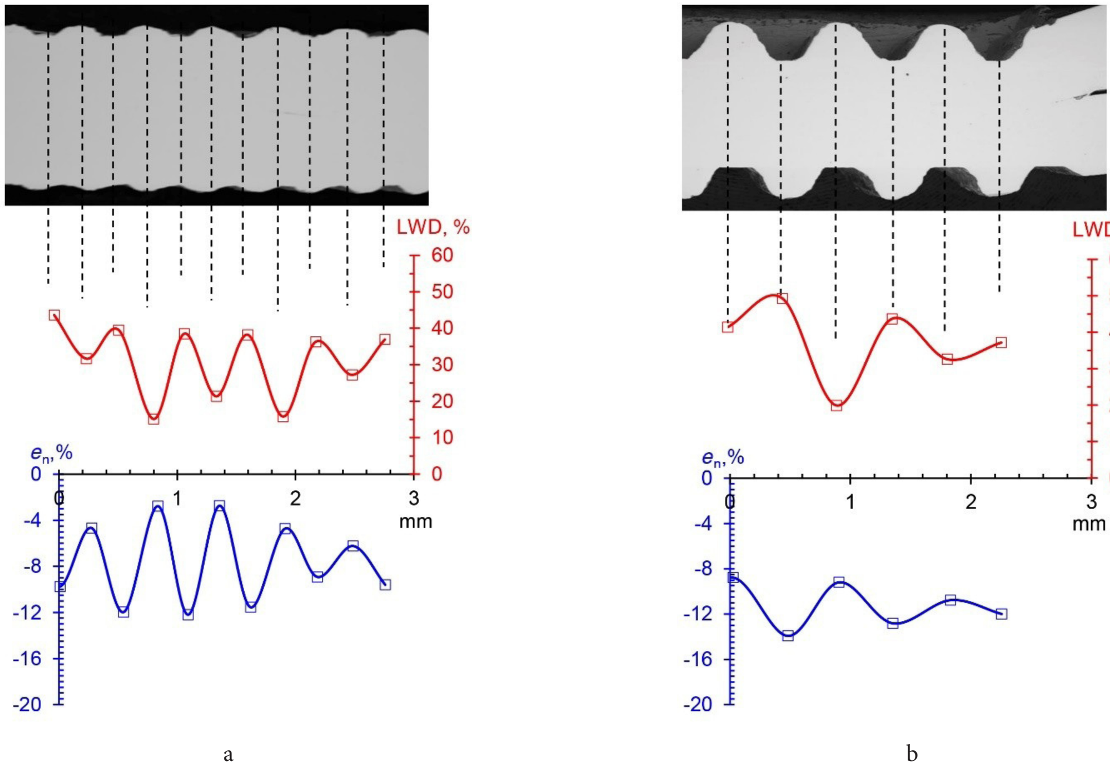

Fig. 3. (Color online) Macrostructures in the cross-sections of samples produced by USW using the tools with the tooth heights of $H=0.1$ mm (a) and $H=0.4$ mm (b) and corresponding distributions of normal strains (blue squares and lines) and linear weld density values (red squares and lines) along joint lines.

3.2. Microstructure

An analysis of the microstructure of the welded specimens showed that, regardless of the height of tool teeth, the joint formation is accompanied by microstructural refinement near contacting surfaces (Fig. 4). This refinement occurred along the entire contact line of plates including the zones near gap-like defects, where the thickness of the fine-grained layer was the smallest. This thickness varied from 3 – 5 μm to 30 – 40 μm after USW with the fine-teeth tool and reached 100 –150 μm with the coarse-teeth one. After USW using the tool with $H=0.4$ mm, spiral vortex patterns formed by fine grains were observed in the joint zone (Fig. 4c, e). At high microscope resolutions (×5000 –15000), pores significantly smaller than 1 μm in size become visible between small grains/subgrains and along the boundaries of the fine-grained layer (Fig. 4d, e), the presence of such pores could not be taken into account when assessing the LWD.

Using the EBSD (orientation) analysis method, a set of maps and quantitative characteristics of the microstructure of the welded samples were obtained (Fig. 5 – 7, Table 2).

Comparing the orientation maps presented in Fig. 5a, b, one can see that after USW using the tools with different tooth heights, microstructures of the samples in joint zones at a distance of approximately 50 μm from the contact surface of the plates, differ dramatically. For the case of the tooth height $H=0.1$ mm, fine-grained regions at interfaces often having a biconvex lens shape neighbored with coarse grains having shapes and sizes similar to those in the initial sheet (Fig. 5a). Within these coarse grains, a developed network of low-angle boundaries (LAB) was observed, the misorientation of which often increased as the fine-grained layer was approached (Fig. 6).

At $H=0.4$ mm, areas consisting of fine equiaxed grains were surrounded by thin elongated grains, the lateral and longitudinal dimensions of which were in ranges 1– 3 μm and 10 – 20 μm, respectively. Together, the fine equiaxed and elongated grains formed swirl-like patterns (Fig. 5b), which are often associated with mechanical interlocking of the metal layers of the plates being joined [3, 4,14, 34].

Figure 7 represents the data on area fractions (a) and frequencies (b) of grains of different sizes in the joint zones outlined by white dotted lines in Figs. 5a and b. It is evident that after USW using the tool with fine teeth, the area of the joint zone occupied by fine grains is nearly half as much than the one after using the coarse-teeth tool (Fig. 7a). Meanwhile, the frequency of the occurrence of grains with a diameter of 0.5 to 2 μm does not depend on the selected tool (Fig. 7b).

Analysis of the structures of fine-grained regions of samples obtained using the ultrasonic tools with tooth heights of $H=0.1$ and 0.4 mm revealed their nearly complete identity (Table 2). In both cases, the fine grains had equiaxed shapes, an average size of 1.1± 0.2 μm, a mean intragranular misorientation of approximately 2° and contained low-angle boundaries (Table 2, Fig. 8).

After USW of copper plates, areas with fine-grained structures have been observed in joint zones in all previous studies known to the authors. At initial stages of ultrasonic welding, when the temperature in the joint zone is less than $(0.3-0.4)T_m$ (see Fig. 2), grain refinement can occur near the contact surfaces due to the development of continuous dynamic recrystallization [35]. At higher temperatures it is

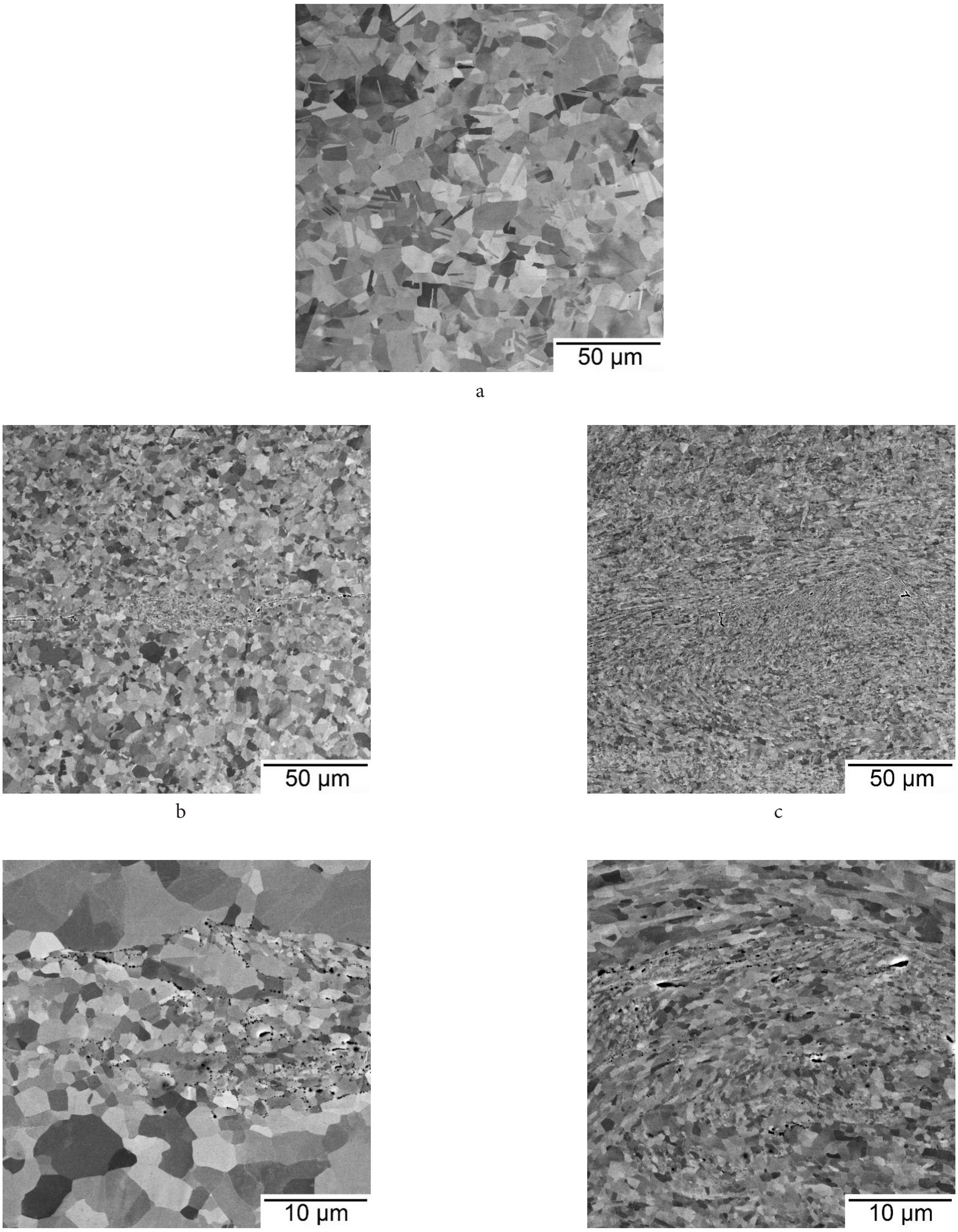

Fig. 4. Typical BSE images of cross sections of the initial copper plate (a) and welded samples produced by USW using the tools with the tooth heights of $H=0.1$ mm (b, d) and $H=0.4$ mm (c, e).

Table 2. Quantitative characterization of the microstructure of samples welded with different tools.

Analyzed region	Height of tool teeth, mm	Mean lineal intercept length, μm		Boundary surface area per unit volume, S_V, μm^{-1}			Mean intragranular misorientation, deg
		Vibration direction	Compression direction	LAB ($2 \le \theta < 15°$)	HAB ($15 \le \theta < 61°$)	Σ3 ($58 < \theta \le 61°$)	
Initial plate		3.9 ± 0.4	3.6 ± 0.4	0.04 ± 0.01	0.57 ± 0.05	0.29 ± 0.03	1.0 ± 0.1
Plate volume	0.1	4.1 ± 0.4	3.4 ± 0.3	0.39 ± 0.04	0.53 ± 0.05	0.13 ± 0.01	2.3 ± 0.2
	0.4	4.6 ± 0.5	2.8 ± 0.3	0.73 ± 0.07	0.55 ± 0.05	0.06 ± 0.01	4.4 ± 0.4
Fine grained region in the joint zone	0.1	1.2 ± 0.2	1.0 ± 0.1	0.76 ± 0.07	1.82 ± 0.11	-	2.1 ± 0.2
	0.4	1.2 ± 0.2	1.1 ± 0.1	0.66 ± 0.07	1.74 ± 0.12	-	2.3 ± 0.3

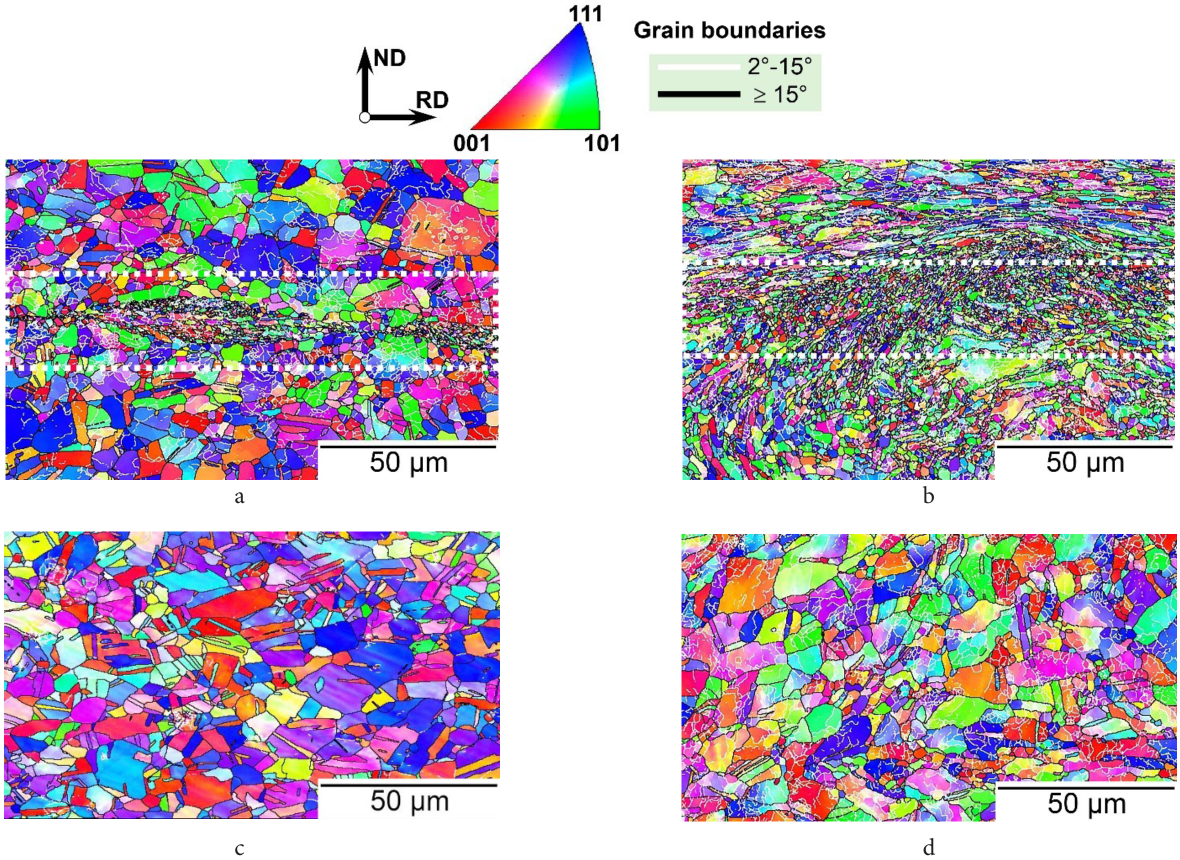

Fig. 5. (Color online) Orientation maps of the microstructure of samples produced by welding using tools with tooth heights of $H = 0.1$ mm (a, c) and $H = 0.4$ mm (b, d); joint zones (a, b [12]), bulks of plates (c, d). The color code is shown over the maps.

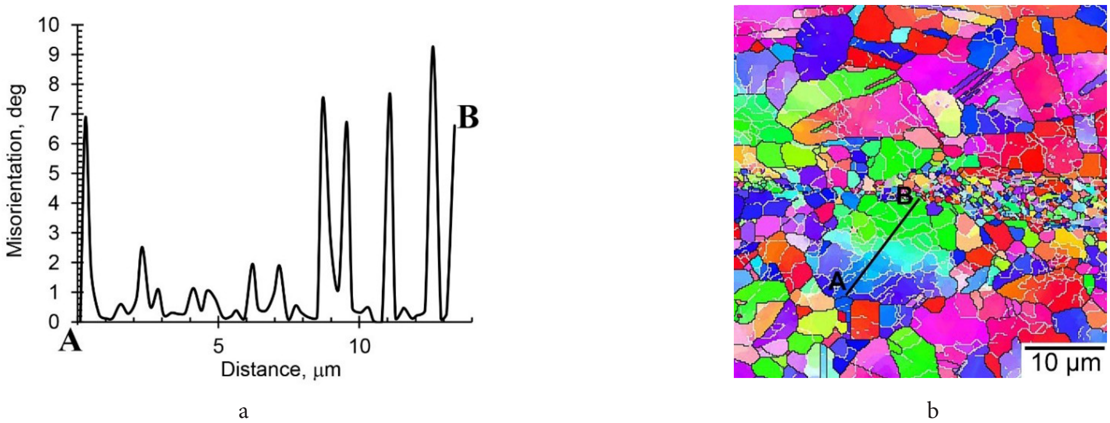

Fig. 6. (Color online) Misorientation profile along line AB (a) and line AB in orientation map (b).

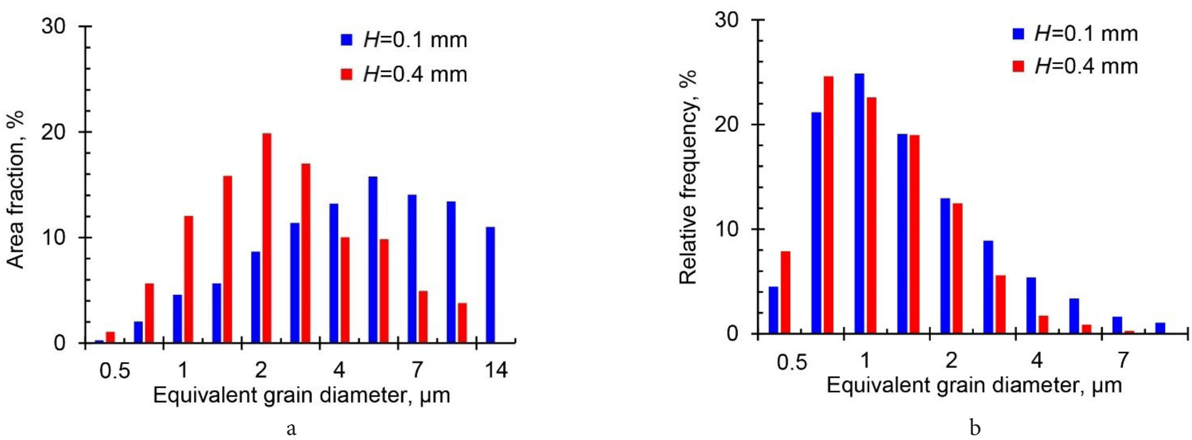

Fig. 7. (Color online) Distributions of grain diameters in the joint zones after USW using different tools: fraction of area (a) and relative frequency (b).

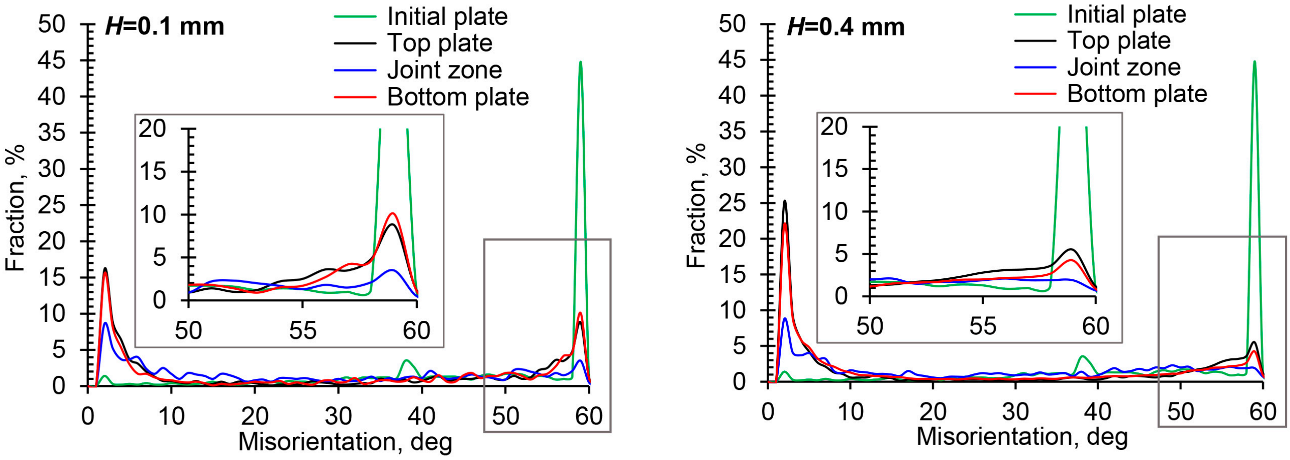

Fig. 8. (Color online) Misorientation angle distributions in different zones of joints produced by USW using the tools with tooth heights of $H=0.1$ mm (a) and $H=0.4$ mm (b) in comparison with corresponding distributions in the initial sheet [29].

more likely that the fine grains form as a result of discontinuous dynamic recrystallization, which is considered as one of the main mechanisms of joint formation during USW [14,18]. Authors of [20,28,36,37] noted that the strongest joints with the lowest number of defects were formed, if migration of grain boundaries across a weld interface occurs, which is accompanied by the grain growth. After USW of dissimilar metals, however, the recrystallization is usually observed only in the softer material, thus diffusion is considered as the main mechanism of joint formation. Furthermore, an important contribution of mechanical interlocking to the strengthening of such (dissimilar) joints is noted [3,4].

In the bulks of the welded plates, both in the top and bottom ones, microstructural changes were caused by the penetration of the tool teeth into the surfaces of the joined plates and the extrusion of metal into the space between the teeth, and were more significant after USW with the tool with coarse teeth (Fig. 5c, d). In the studied areas located at a distance of about 100 μm from the contact surface, the shapes and sizes of grains were close to those in the initial sheet. However, boundary misorientation spectra changed significantly as compared to the initial material (Fig. 8, Table 2). Substructure was formed in the bulks of the plates, as evidenced by the appearance of peaks in the misorientation range of 2–15° (Fig. 8). After welding with the fine- and coarse-teeth tools, the specific length of LAB demonstrated 10- and 20-fold increases, respectively, as compared to the initial material (Table 2). The substructure formation was accompanied by an increase in the average intragranular misorientation (Table 2), which is explained by an increased density of dislocations of the same sign within the grains (geometrically necessary dislocations). Metal flow within the bulks of the plates violated the structure of twin boundaries transforming them into random grain boundaries with misorientation angles about 55–58°. This is evidenced by a sharp decrease in the height and spreading of the peak at 60° (inserts in Fig. 8a, b). Compared to the initial state, the surface area per unit volume of twin boundaries Σ3 decreased by factors of 2 and 5 after USW with the tools with fine and coarse teeth, respectively (Table 2).

The observed differences in microstructures of the samples welded with different tools did not affect significantly

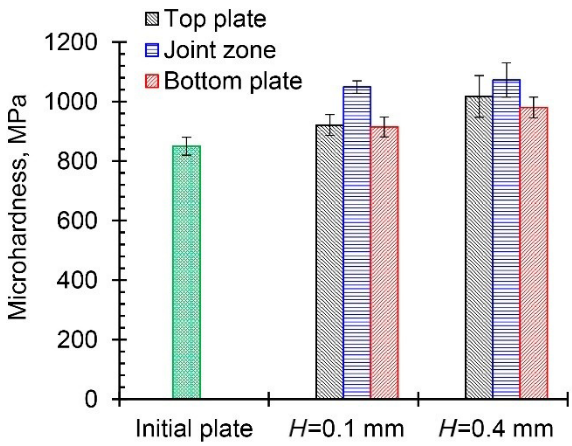

Fig. 9. (Color online) Microhardness in different zones of welded samples of the Cu/Cu joints produced by the USW with a tool with different tooth heights.

their microhardness, which increased slightly in both cases compared to the initial state (Fig. 9a), and the fracture loads of the specimens. The average failure loads during lap-shear tests of samples USW-ed using the fine- and coarse-teeth tools were equal to 2075±100 and 1918±241 N, respectively, and did not differ within the statistical dispersion of the experimental data. Meanwhile, the value of standard deviation of the failure loads was by a factor of 2.4 smaller after USW with the tool with tooth size of $H=0.1$ mm.

An increase in the strength of joints produced by the tool with height $H=0.4$ mm which might be expected due to mechanical interlocking was, probably, compensated by the increase in the distance between the areas having large (approximately 40%) LWDs (Fig. 3). Such areas, which are microbonds, form primarily under the imprints of the tip teeth, which is confirmed by the results of fractographic studies [38]. Therefore, the distance between them is determined by the distance between the teeth of the welding tip, which is half as much when using the tool with fine teeth. It should be emphasized that reducing the height of the tool teeth from 0.4 to 0.1 mm led to a decrease in the average LWD by only 6%. Moreover, after USW with the tool with fine teeth, areas with a LWD of approximately 40% were observed twice as often as after USW with the tool with coarse teeth (Fig. 3). For this reason, using the tool with 0.1 mm teeth not only preserved the strength properties of the joints but also reduced the coefficient of variation in fracture loads from 12% after USW with the tool with large teeth to 5%. It is worth noting that changing the surface shape of the welding tip from a flat to spherical [11] or cylindrical one [10] reduced the coefficient of variation in fracture loads for the strongest joints from 20–35% to 17–10%. Thus, optimizing the height of the knurls on the surface of a flat welding tool is an effective method for improving the stability of welded joints.

4. Conclusions

In this study, USW using tools with tooth heights of 0.1 and 0.4 mm was used to produce spot welds of 0.8 mm-thick copper plates. All welding parameters (frequency, amplitude, clamping pressure, time) and the welding tip area were identical. Assessments of the influence of tool tooth height on the distribution of normal compressive strains at the weld spot and the distribution of the linear weld density, as well as on the microstructure and strength characteristics of the welded samples, revealed the following:

1. Local compressive strains at the weld spot vary periodically. The period of their variation is equal to the distance between the tip teeth and is half as much after USW with the tool with fine teeth than after USW with the tool with coarse teeth. The highest compressive strains of 12–14% are achieved under the tip tooth imprints and are independent of their height, so is the linear welding density of the joints, which amounts approximately 40% under the tip tooth imprints.

2. Regardless of the welding tool used, USW results in the formation of a fine-grained structure at the joint interfaces due to dynamic recrystallization. At high resolutions of a microscope, submicrometer-sized pores are detected between the fine grains.

3. USW using a tool with a tooth height of 0.4 mm is accompanied by mechanical interlocking. In areas of mechanical interlocking, small equiaxed grains and elongated deformed grains form swirl-like patterns.

4. The indentation of the tool teeth into the plates under joining and the extrusion of metal between the teeth lead to the formation of low-angle boundaries and violation of the structure of twin boundaries within the welded plates. The specific length of low-angle boundaries is significantly larger and the number of twin boundaries is smaller after USW with the tool with the height of teeth $H = 0.4$ mm.

5. The average fracture loads of welded samples obtained using the tools with different tooth heights are similar and amount to approximately 2000 N. However, the variation coefficient of the test results is by a factor of 2.4 smaller after ultrasonic welding using the tool with fine teeth. We assume that the increase in the stability of test results is due to a twofold reduction in the distance between areas with acceptable linear density after ultrasonic welding with the fine tool. Thus, optimizing the knurl height of flat welding tools can be an effective method for improving the stability of properties of ultrasonically welded joints.

References

1. P.R. Vishnu, Solid-state transformations in weldments, in: D.L. Olson, T.A. Siewert, S. Liu, G.R. Edwards (Eds.), ASM Handbook Welding, brazing, and soldering, Materials park, ASM International, 1998, pp. 177–229.
2. M.J. Cieslak, Cracking phenomena associated with welding, in: D.L. Olson, T.A. Siewert, S. Liu, G.R. Edwards (Eds.), ASM Handbook, Welding, brazing, and soldering, Materials park, ASM International, 1998, pp. 229–248.
3. M. de Leon, H.S. Shin, Review of the advancements in aluminum and copper ultrasonic welding in electric vehicles and superconductor applications, J. Mater. Process. Technol. 307 (2022) 117691.
4. J. Yang, C. Xie, J. Zhang, J. Qiao, Design strategies for enhancing strength and toughness in ultrasonic welding of dissimilar metals: A review, Mater. Today Commun., 42 (2025) 111502.
5. E.B. Schwarz, F. Bleier, F. Guenter, R. Mikut, J.P. Bergmann, Improving process monitoring of ultrasonic metal welding using classical machine learning methods and process-informed time series evaluation, J. Manuf. Process. 77 (2022) 54–62.
6. F.W. Müller, A. Schiebahn, U. Reisgen, Quality prediction of disturbed ultrasonic metal welds, J. Adv. Join. Process., 5 (2022) 100086.
7. F.W. Müller, C. Mirz, S. Weil, A. Schiebahn, B. Corves, U. Reisgen, Weld quality characterization by vibration analysis for ultrasonic metal welding processes, J. Adv. Join. Process. 8 (2023) 100149.
8. D. Zhao, C. Zhang, Z. Peng, Y. Xu, C. Zhang, Ultrasonic welding of copper alloys: a review, Sci. Technol. Weld. Join. 30 (2025) 399–434.
9. T. Sasaki, Y. Sakata, T. Watanabe, Effect of tool geometry on ultrasonic welding process, IOP Conf. Ser.: Mater. Sci. Eng., 61 (2014) 012006.
10. T. Watanabe, D. Miyajima, A. Yanagisawa, Effect of weld tip geometry on ultrasonic welding of A6061 aluminium alloy, Weld. Int. 24 (2010) 336–342.
11. L. Nong, C. Shao, T.H. Kim, S.J. Hu, Improving process robustness in ultrasonic metal welding of lithium-ion batteries, J. Manuf. Syst. 48 (2018) 45–54.
12. M.A. Murzinova, E.R. Shayakhmetova, A.A. Mukhametgalina, A.A. Sarkeeva, A.A. Nazarov, Local plastic deformation and quality of Cu-Cu joints obtained by ultrasonic welding, Metals 13 (2023) 1661.
13. D. Zhao, C. Jiang, K. Zhao, Ultrasonic welding of AZ31B magnesium alloy and pure copper: microstructure, mechanical properties and finite element analysis, J. Mater. Res. Technol. 23 (2023) 1273–1284.
14. Z. Su, Z. Zhu, Y. Zhang, H. Zhang, Q. Xiao, Recrystallization behavior of a pure Cu connection interface with ultrasonic welding, Metals 11 (2020) 61.
15. H. Huang, J. Chen, Y.C. Lim, X. Hu, J. Cheng, Z. Feng, X. Sun, Heat generation and deformation in ultrasonic welding of magnesium alloy AZ31, J. Mater. Process. Technol. 272 (2019) 125–136.
16. Y. Lu, H. Song, G.A. Taber, D.R. Foster, G.S. Daehn, W. Zhang, In-situ measurement of relative motion

during ultrasonic spot welding of aluminum alloy using photonic doppler velocimetry, J. Mater. Process. Technol. 231 (2016) 431 – 440.
17. I. Balz, E. Raad, E. Rosenthal, R. Lohoff, A. Schiebahn, U. Reisgen, M. Vorländer, Process monitoring of ultrasonic metal welding of battery tabs using external sensor data, J. Adv. Join. Process. 1 (2020) 100005.
18. Q. Ma, J. Ma, J. Zhou, H. Ji, Intrinsic dependence of welding quality and recrystallization on the surface-contacted micro-asperity scale during ultrasonic welding of Cu-Cu joints, J. Mater. Res. Technol. 17 (2022) 353 – 364.
19. L.L. Silin, G.F. Balandin, M.G. Kogan. In: Ultrasonic Welding: Joining of Metals in Solid State and Improvement of Quality of Welds (ed. by N.N. Rykalin), Moscow, Mashgiz (1962) pp. 25 – 64. (in Russian)
20. F. Haddadi, D. Tsivoulas, Grain structure, texture and mechanical property evolution of automotive aluminium sheet during high power ultrasonic welding, Mater. Charact. 118 (2016) 340 – 351.
21. N. Shen, A. Samanta, W. Cai, T. Rinker, B. Carlson, H. Ding, 3D finite element model of dynamic material behaviors for multilayer ultrasonic metal welding, J. Manuf. Process. 62 (2021) 302 – 312.
22. E.R. Shayakhmetova, M.A. Murzinova, A.A. Mukhametgalina, A.A. Nazarov, Structure evolution in ultrafine-grained nickel induced by ultrasonic welding, Lett. Mater. 14 (2024) 91 – 96.
23. M. Feng, Z. Luo, Interface morphology and microstructure of high-power ultrasonic spot welded Mg/Al dissimilar joint, Sci. Technol. Weld. Join. 24 (2019) 63 – 78.
24. R. Jahn, R. Cooper, D. Wilkosz, The effect of anvil geometry and welding energy on microstructures in ultrasonic spot welds of AA6111-T4, Met. Mater. Trans. A 38 (2007) 570 – 583.
25. H. Shin, M. de Leon, Parametric study in similar ultrasonic spot welding of A5052-H32 alloy sheets, J. Mater. Process. Technol. 224 (2015) 222 – 232.
26. Z. Ma, Y. Zhang, Characterization of multilayer ultrasonic welding based on the online monitoring of sonotrode displacement, J. Manuf. Process., 54 (2020) 138 – 147.
27. F. Ye, Y. Wang, H. Lu, Y. Guo, Study on the bonding mechanism of multilayer copper with nickel sheet in ultrasonic welding process, Mater. Res. Express 9 (2022) 026527.
28. J. Yang, B. Cao, Q. Lu, The effect of welding energy on the microstructural and mechanical properties of ultrasonic-welded copper joints, Materials 10 (2017) 193.
29. A.A. Mukhametgalina, E.R. Shayakhmetova, M.A. Murzinova, A.A. Nazarov, A.A. Sarkeeva, Effect of surface state on the quality of copper joints produced by ultrasonic welding, Lett. Mater. 14 (2024) 190 – 197.
30. M.A. Murzinova, E.R. Shayakhmetova, A.A. Mukhametgalina, A.A. Nazarov, Microstructure of multilayer sample produced by sequential ultrasonic welding of ultrafine-grained nickel, Weld. World (2025).
31. F.J. Humphreys, M. Hatherly, Recrystallization and Related Annealing Phenomena, UK, 2004, 628 p.
32. T. Sakai, A. Belyakov, R. Kaibyshev, H. Miura, J. Jonas, Dynamic and post-dynamic recrystallization under hot, cold and severe plastic deformation conditions, Prog. Mater. Sci. 60 (2014) 130 – 207.
33. H. Li, B. Cao, J. Liu, J. Yang, Modeling of high-power ultrasonic welding of Cu/Al joint, Int. J. Adv. Manuf. Technol. 97 (2018) 833 – 844.
34. D. Bakavos, P.B. Prangnell, Mechanisms of joint and microstructure formation in high power ultrasonic spot welding 6111 aluminium automotive sheet, Mater. Sci. Eng.: A 527 (2010) 6320 – 6334.
35. J.Y. Lin, Z.H. Lai, T. Otsuki, H.W. Yen, S. Nambu, Gradient microstructure and interfacial strength of CoCrFeMnNi high-entropy alloy in solid-state ultrasonic welding, Mater. Sci. Eng.: A 825 (2021) 141885.
36. A.A. Ward, M.R. French, D.N. Leonard, Z.C. Cordero, Grain growth during ultrasonic welding of nanocrystalline alloys, J. Mater. Process. Technol. 254 (2018) 373 – 382.
37. P. Li, Z. Wang, M. Diao, C. Guo, J. Wang, C. Zhao, F. Jiang, Effect of processing parameters on bond properties and microstructure evolution in ultrasonic additive manufacturing (UAM), Mater. Res. Express. 8 (2021) 036507.
38. E.R. Shayakhmetova, Strength of joints produced by ultrasonic spot welding of copper plates using tools with different tooth heights, Front. Mater. & Technol. 3 (2025) 125 – 136.